Electronic Supplementary Material (ESI) for Soft Matter.
This journal is © The Royal Society of Chemistry 2017

Characterizing the Tilt Angle and Aggregation of Gold Nanorod Polymer Nanocomposites

Supporting Information

Sample Details

Sample	Matrix Polymer	Brush Polymer	Percent Loading	Initial Film Thickness (nm)	*S* (Initial)	Film Thickness After 5 hr at 473 K (nm)	*S* (after 5hrs at 473 K)	Film Thickness After 24 at 473 K (nm	Relevant Figure numbers
PS/PS	PS, M_n=5.3 kg/mol	PS, M_n=11.5 kg/mol	4%	65±0.2	-0.29 at 742 nm	65±0.2	0 at 629 nm	55 ±0.2	6, S4, S5, and S7, S8
PMMA/PS	PMMA, M_n=1.1 kg/mol	PS, M_n=11.5 kg/mol	4%	73 ±0.2	-0.32 at 747 nm	N/A	N/A	N/A	1-5, S1, S3, and S6
PMMA/PS(2)	PMMA, M_n=1.1 kg/mol	PS, M_n=11.5 kg/mol	4%	62 ±0.2	-0.26 at 722 nm	62 ±0.2	-0.1 at 615 nm	62 ±0.2	6 and S7, S8

Table S1: Details of the Polymer/AuNR nanocomposite samples.

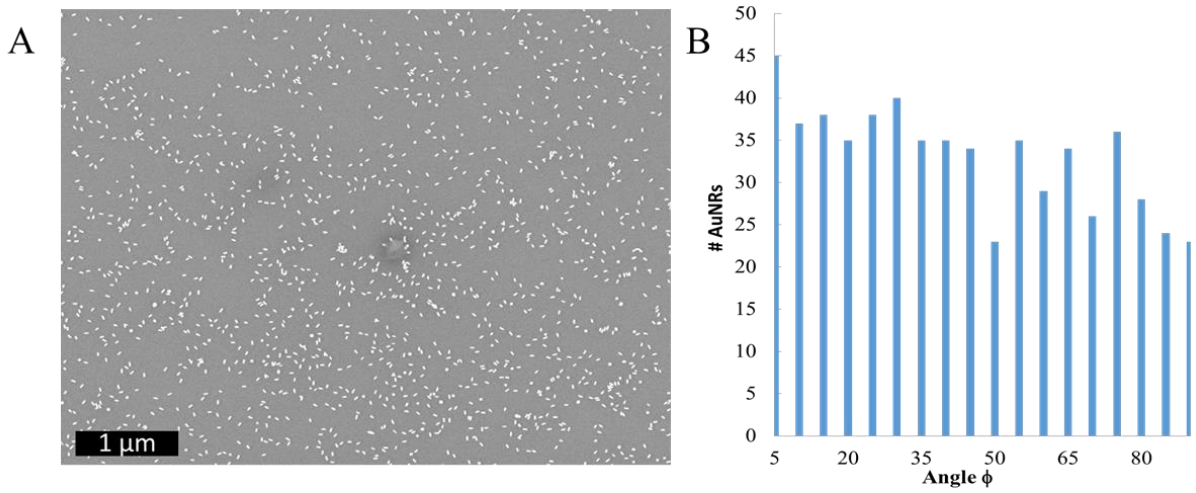

Figure S1. A) Large area SEM image of the PMMA/PS sample with 4% loading of AuNRs. B) Histogram of AuNR in-plane angles (ϕ) where at 90° the AuNR is pointing directly in the *y* direction and at 0° the AuNR is pointing in the *X* direction. The histogram shows uniform in-plane orientation of the rods.

Ellipsometry Details

The measured ellipsometry parameter profiles (Ψ(λ) and Δ(λ)) were used to obtain the optical constants of the composite film through several fitting procedures using a two-layer model. A Cauchy model with known coefficients for BK7 glass was used for the substrate layer. (Glass, instead of silicon, was used for ellipsometry measurements to prevent the scattering from nanorods being masked by substrate reflection.) For the composite layer, all fits began with fitting the transparent region of the composite film (1000-1600 nm) to the Cauchy equation $n(\lambda) = A + \frac{B}{\lambda^2} + \frac{C}{\lambda^4}$ in order to characterize the thickness of the film, which was determined to be 73 nm for a nanocomposite film of AuNRs grafted with 11 kg/mol PS in a 1 kg/mol PMMA film. Fitting this region allows us to fit the thickness of the film independently of the plasmon excitations of the nanorods. Then, the fit was extended to lower wavelengths, where the material is absorbing through an isotropic wavelength-by-wavelength, which was set to be Kramers-Kronig consistent[1]. This brute force method fits an independent value for the complex dielectric constant at each wavelength. To reduce the number of independent variables and fit the optical constants of the nanocomposite film, the L-LSPR and T-LSPR resonances were fit with a series of oscillators.

It was observed that a number of five Gaussian oscillators were required to accurately represent the dielectric constants (parameters detailed in table S1). The five oscillators can generally be split into two categories, three that fit the L-LSPR and T-LSPR peaks, and two that fit the general properties of gold at low wavelengths (λ < 500 nm). The L-LSPR peak is naturally broad due to the size distribution of the nanorods, and thus this peak was fit with two Gaussian oscillators. The T-LSPR is much weaker, so it was fit with a single Gaussian oscillator with a large breadth in order to encompass the size distribution of the width of the nanorods. One could stop here. The difference between the isotropic and anisotropic fit in Figure S4 is an example of a three oscillator fit, which can show a drastically increased fit quality upon the

addition of anisotropy. This is sample dependent, however. If there happens for whatever reason to be a weaker signal, then the T-LSPR can merge into the general optical properties of gold at wavelengths $\lambda < 500$ nm. When this happens, the T-LSPR peak broadens and interferes with the fit for the L-LSPR. This can result in unphysical fits (ie. Oscillators with unreasonable parameters or unphysical anisotropy results).

To avoid this problem, two additional oscillators were added to each fit to describe the general optical properties of gold at $\lambda < 500$ nm. While we have limited sensitivity when $\lambda < 450$ nm, the addition of these oscillators leaves the oscillators representing the L-LSPR modes unperturbed when anisotropy is added to the model. To avoid over fitting the data upon the addition of anisotropy, the two oscillators at $\lambda < 500$ nm (including the T-LSPR) were locked to their isotropic values. An anisotropic fit with the five oscillator model does not show as large a decrease in MSE in comparison to the isotropic fit, but the fit still improves by more than 15% for every sample, signifying a real change in the fit quality.

Table S2: Oscillator Parameters For the Fit in Figure 2 (

Oscillator Type	**Amplitude**	**Breadth**	**Energy (eV)**	**Wavelength (nm)**
Gaussian	0.128361	0.2898	1.709	725
Gaussian	0.175989	0.2231	1.654	750
Gaussian	0.079855	1.1096	2.164	573
Gaussian	0.046290	0.5333	3.001	413
Gaussian	0.037028	0.2484	3.296	376

Simulation Description

Finite-difference time-domain (FDTD) simulations were performed using the commercial software Lumerical FDTD Solutions (Version 8.11). Details in the simulation setup have been described in our previous publications.[2, 3] In a typical simulation, a single AuNR was modelled as cylinder with two semi-spherical ends, with a refractive index profile of gold obtained from the CRC Handbook of Chemistry & Physics[4]. The length and diameter of the rod was extracted from SEM images and set to 34 nm and 12 nm, respectively. The size was verified by comparing the simulated far-field extinction spectrum with the experimental UV-Vis results. The model was then excited by a 1.33 fs broadband total-field scatter-field (TFSF) pulse source of unit amplitude with a background index of 1.49, mimicking the PMMA matrix, and perfectly matched layer (PML) boundary conditions in all dimensions.

The simulated frequency-domain electric near-field distribution was used to calculate the induced dipole moment $\boldsymbol{p}$ and the corresponding polarizability α according to the following equation, where $\boldsymbol{E_0}$ and n_b are the incident electric field and background refractive index, respectively[5]:

$$\boldsymbol{p} = \alpha \boldsymbol{E_0} = \frac{i}{\omega} \int \varepsilon_0 (n^2 - n_b^2) \boldsymbol{E}\, dV$$

Under the dipole approximation, the calculated single rod polarizability can be used to describe the effective refractive index of a composite with a uniform orientation of nanorods, using the Clausius-Mossotti relation where N is the number density of dipoles[6]:

$$n_{eff} = \left(\frac{1 + \frac{2N}{3\varepsilon_0}\alpha}{1 - \frac{N}{3\varepsilon_0}\alpha} \right)^{\frac{1}{2}}$$

As shown in Fig. S1, two effective index values, one each for the L-LSPR ($n_l = N_{L-LSPR} + iK_{L-LSPR}$) and T-LSPR ($n_t = N_{T-LSPR} + iK_{T-LSPR}$) modes can be calculated from the above method using near-field data under incident polarization parallel and perpendicular to the rod, respectively, and assuming an average dipole number density of $N = \frac{1}{(60)^3}$ nm^{-3}. The effective indices were used to calculate the effective uniaxial birefringent optical properties, given the fact that the rods demonstrate a random in-plane orientation and a relatively small out-of-plane tilt. Details of this method will be published elsewhere.

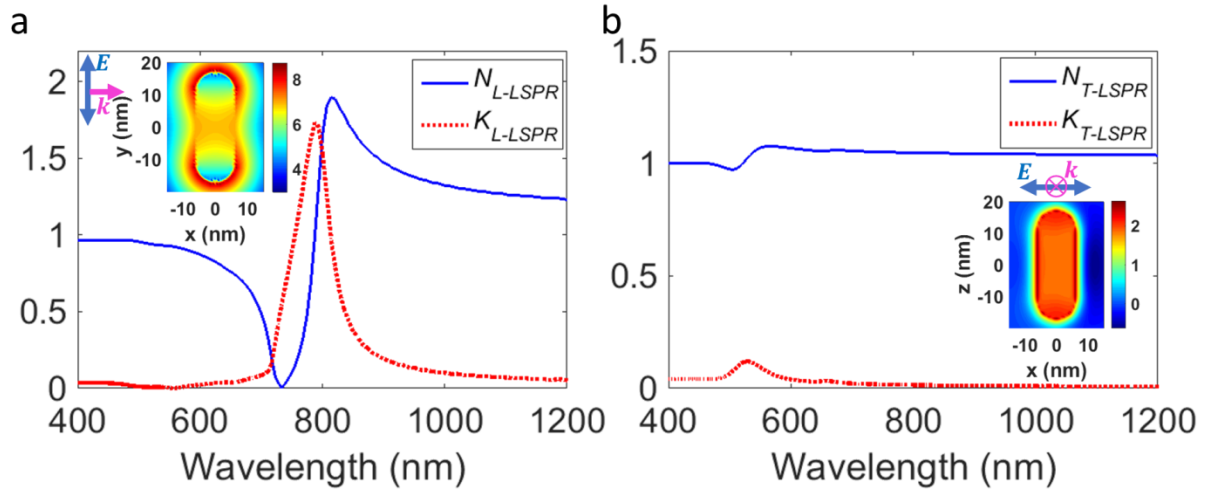

Figure S2. Effective refractive index calculations for L-LSPR (a) and T-LSPR (b) modes based on FDTD simulation of a single AuNR and Clausius-Mossotti relation. Insets show the near-field intensity distribution around the modelled AuNR at the resonance wavelength (764 nm for L-LSPR and 520 nm for T-LSPR) with corresponding incident polarization directions.

Under oblique incidence, a composite medium with a uniform AuNR orientation can be calculated as follows, where α is the angle between a rod and the incident electric field:

$$\frac{1}{n^2} = \frac{\sin^2\alpha}{n_l^2} + \frac{\cos^2\alpha}{n_t^2}$$

Then the uniaxial refractive indices of the actual composite can be calculated as an average over a specific range of angles. It should be noted that the angle α between the rod orientation and incident electric field can be related to the angle θ between the rod orientation and the composite film surface normal ($\hat{\boldsymbol{z}}$) by $\cos\alpha = \sin\theta\sin\phi$ for the in-plane incident

polarization (*y*-polarization was assumed since in-plane orientation is arbitrary) and $\alpha = \theta$ for the out-of-plane incident polarization, where ϕ is the angle between the *x* axis and the *xy*-plane projection of the rod orientation. The effective refractive indices can then be calculated as:

$$\frac{1}{n_{xy}^2} = \frac{< 1 - \sin^2\theta \sin^2\phi >}{n_l^2} + \frac{< \sin^2\theta \sin^2\phi >}{n_t^2}$$

$$\frac{1}{n_z^2} = \frac{< \cos^2\theta >}{n_l^2} + \frac{< \sin^2\theta >}{n_t^2}$$

More detailed analysis of the effective-medium calculations are outside the scope of this paper will be presented in our future publications.

A)

B)

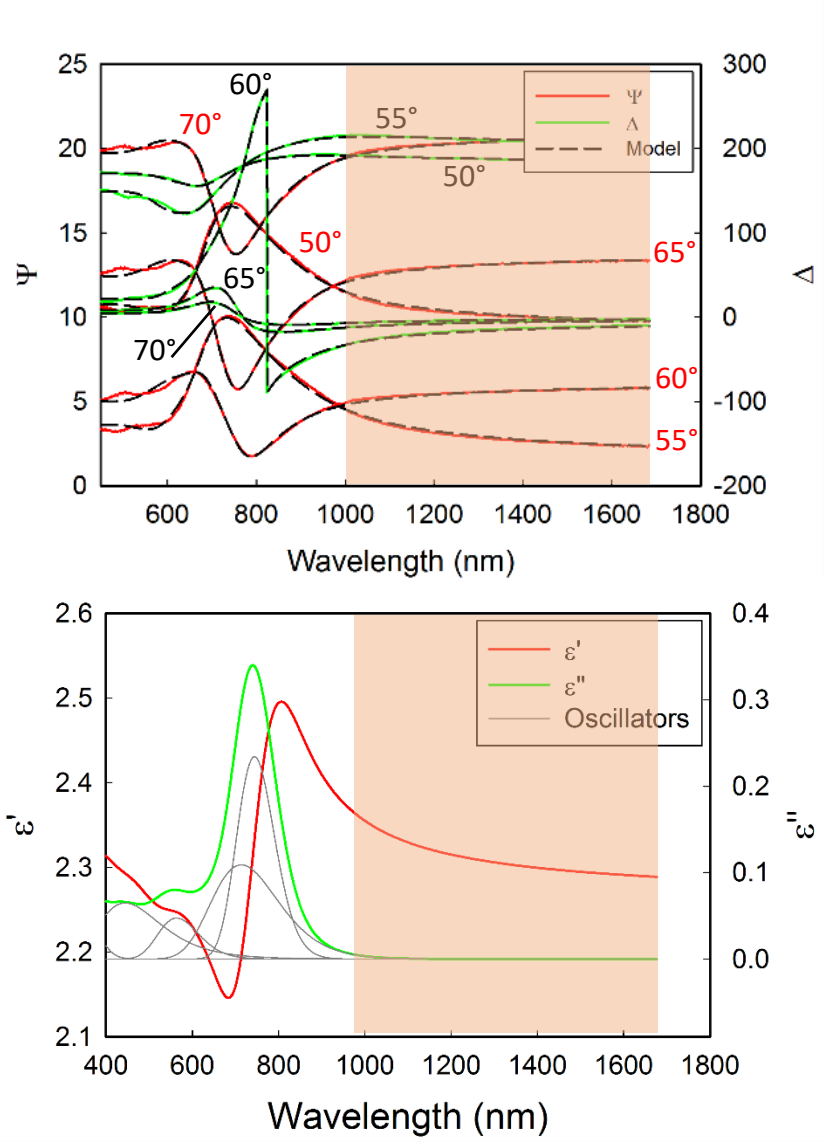

Figure S3: A) Ellipsometric angles Ψ (red) and Δ (green) data vs. wavelength for the PMMA/PS sample at five angle of incidence (50°, 55°, 60°, and 65°, and 70° degrees), along with the corresponding two-layer isotropic model (black dashed line) used to simultaneously fit to all data points for both Ψ and Δ in the wavelength range of 400-1600nm. The data in the range of 1000 nm-1600 nm was fit to a transparent Cauchy model. The fit was then extended to lower wavelength range (1000 nm down to 400 nm) using a Kramers-Kronig consistent model. B) The resulting calculated real (ε', red line) and imaginary (ε", green line) parts of dielectric permittivity as a function of wavelength. The gray curves represent the five Gaussian oscillators used to determine ε" (green line), while ε' (red line) was determined via a Kramers-Kroning transformation of the determined ε". Film thickness is measured to be 73 ±0.2 nm based on this fit.

A)

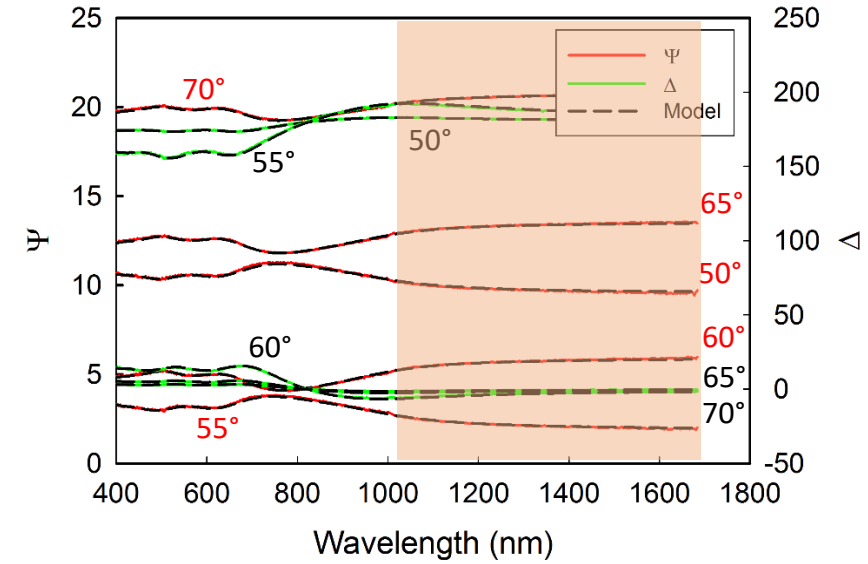

B)

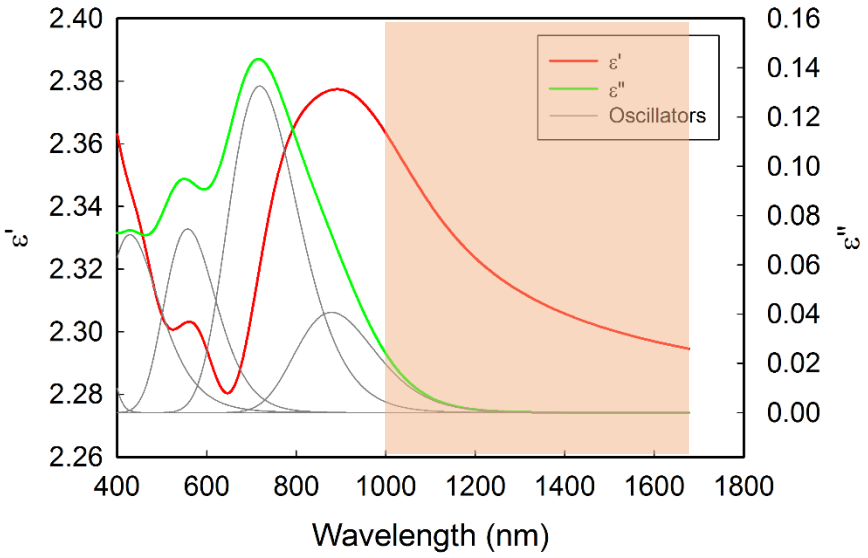

Figure S4. a) Ellipsometric angles Ψ (red) and Δ (green) data vs. wavelength for the PS/PS sample at five angle of incidence (50°, 55°, 60°, and 65°, and 70° degrees), along with the corresponding two-layer isotropic model (black dashed line) used to simultaneously fit to all data points for both Ψ and Δ in the wavelength range of 400-1600nm. The data in the range of 1000 nm-1600 nm was fit to a transparent Cauchy model. The fit was then extended to lower wavelength range (1000 nm down to 400 nm) using a Kramers-Kronig consistent model. b) The resulting calculated real (ε', red line) and imaginary (ε", green line) parts of dielectric permittivity as a function of wavelength. The gray curves represent the five Gaussian oscillators used to determine ε" (green line), while ε' (red line) was determined via a Kramers-Kroning transformation of the determined ε"

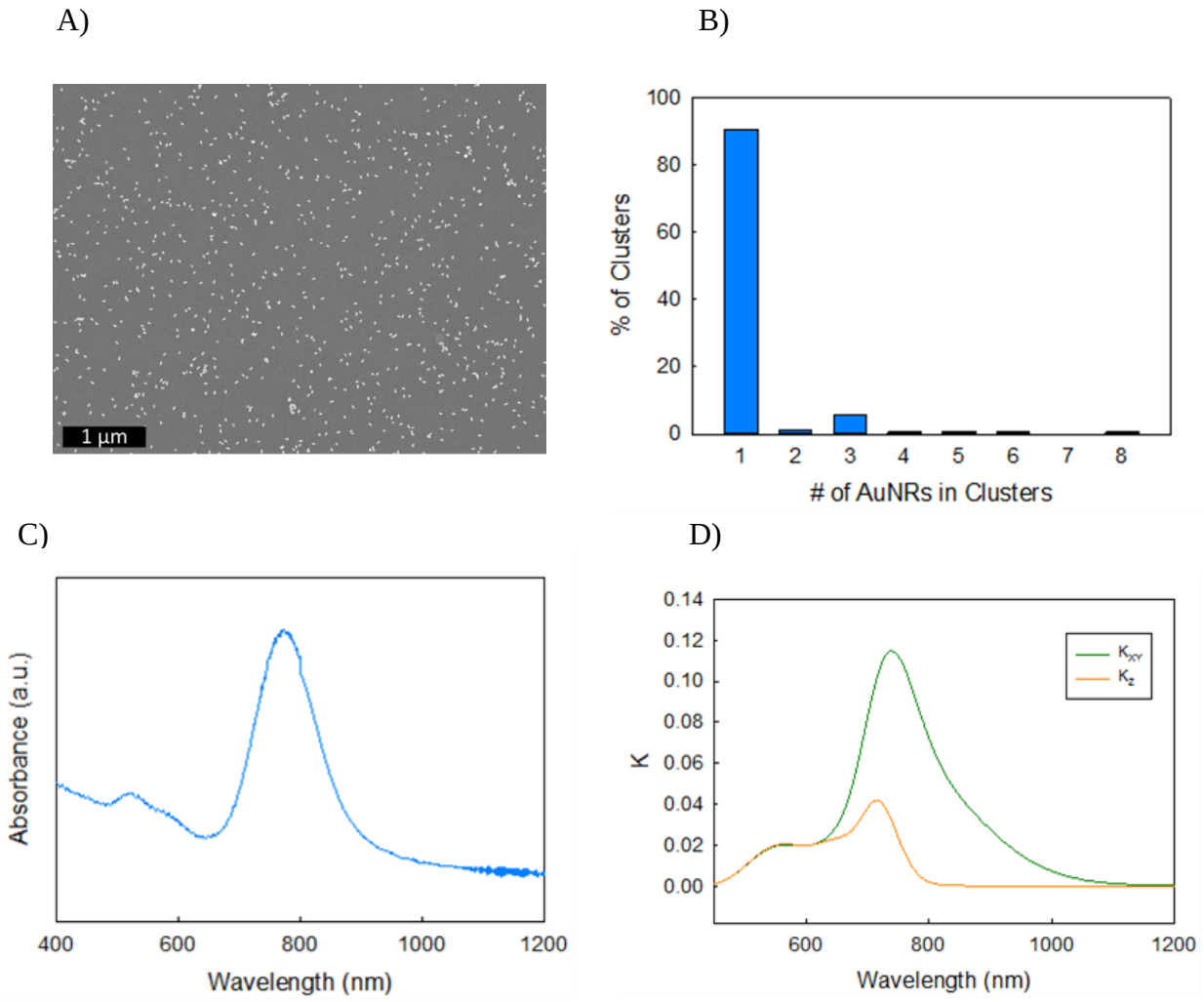

Figure S5: PS/PS sample 65 nm ± 0.2 thick characterized by A) SEM imaging B) Cluster Analysis C) optical absorption spectroscopy, and D) Ellipsometry. The orientation order parameter of this sample is determined to be -0.29 at 742 nm.

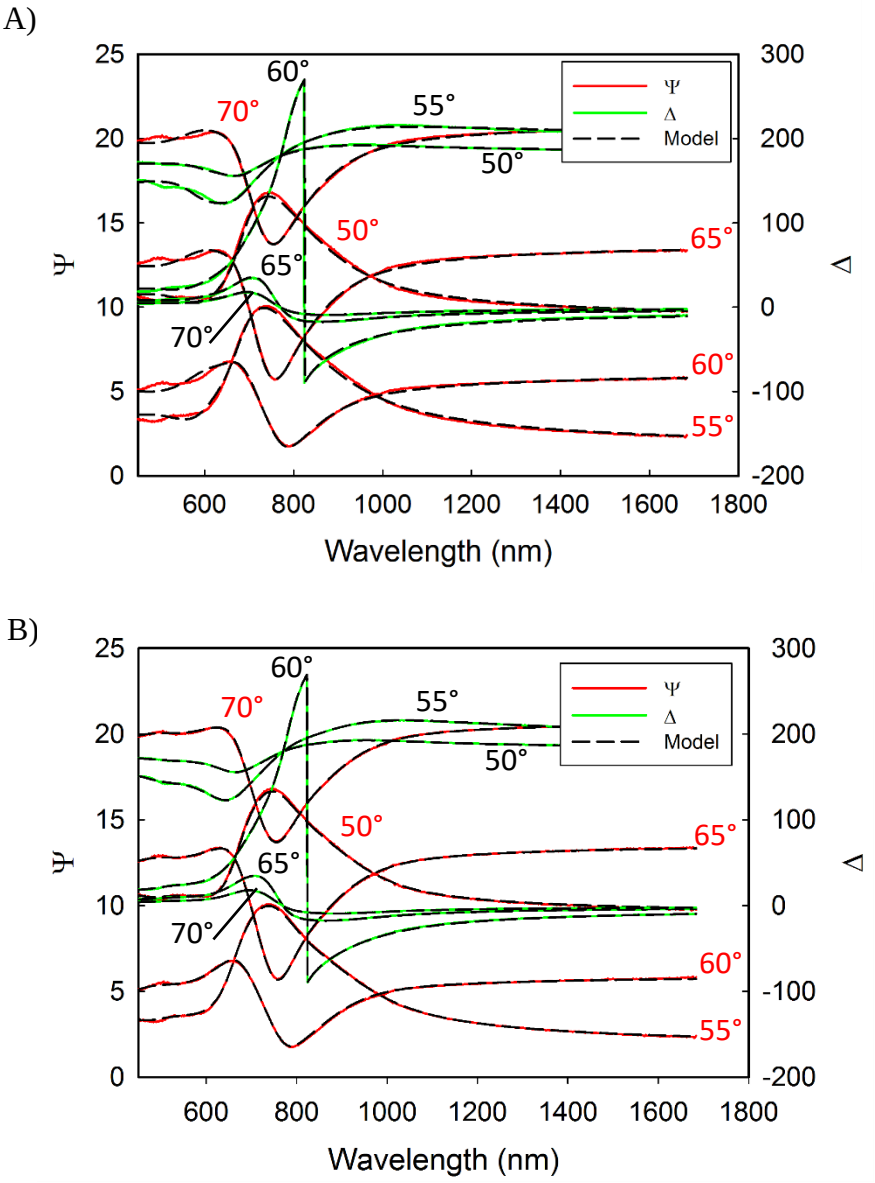

Figure S6: Ellipsometry fits of the PMMA/PS sample using A) an Isotropic fit with an MSE of 4.1 and B) An anisotropic fit with an MSE of 1.3. The incident angles of Ψ(λ) and Δ(λ) are labeled by red and black numbers, respectively. All fits began by fitting the transparent region (1000-1600 nm) to the Cauchy equation $n(\lambda) = A + \frac{B}{\lambda^2} + \frac{C}{\lambda^4}$ in order to characterize the thickness of the film. Then, the fit was extended through the rest of the spectral range with an isotropic wavelength-by-wavelength BSpline fit. The resulting optical constants were then parameterized to a series of oscillators. B) Anisotropy was added to the model after the oscillators were parameterized in the manner mentioned above.

A)

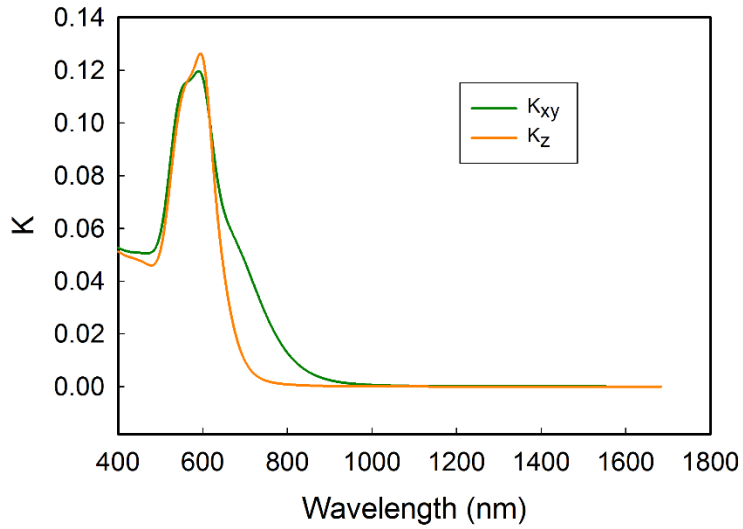

B)

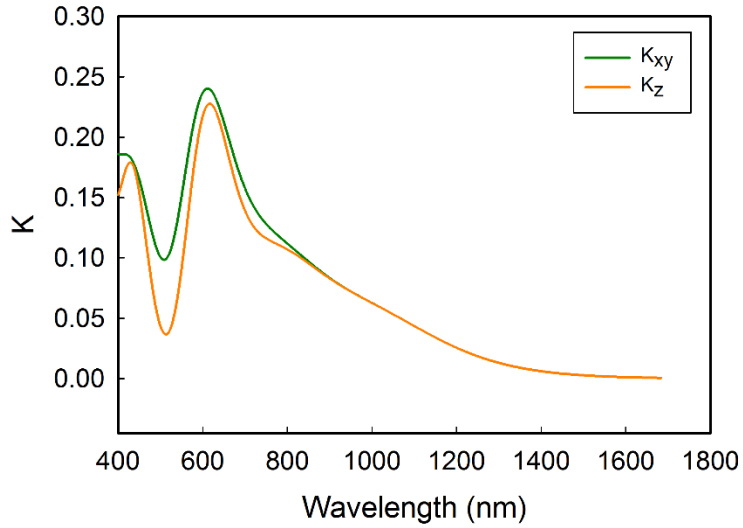

Figure S7: Anisotropic absorbance of A) PMMA/PS(2) and B) PS/PS sample, after being annealed at 473 K for 24 hours. The final film thicknesses are measured to be 65 ±0.2 nm and 55 ±0.2 nm, respectively. Both samples are isotropic after 24 hrs of annealing.

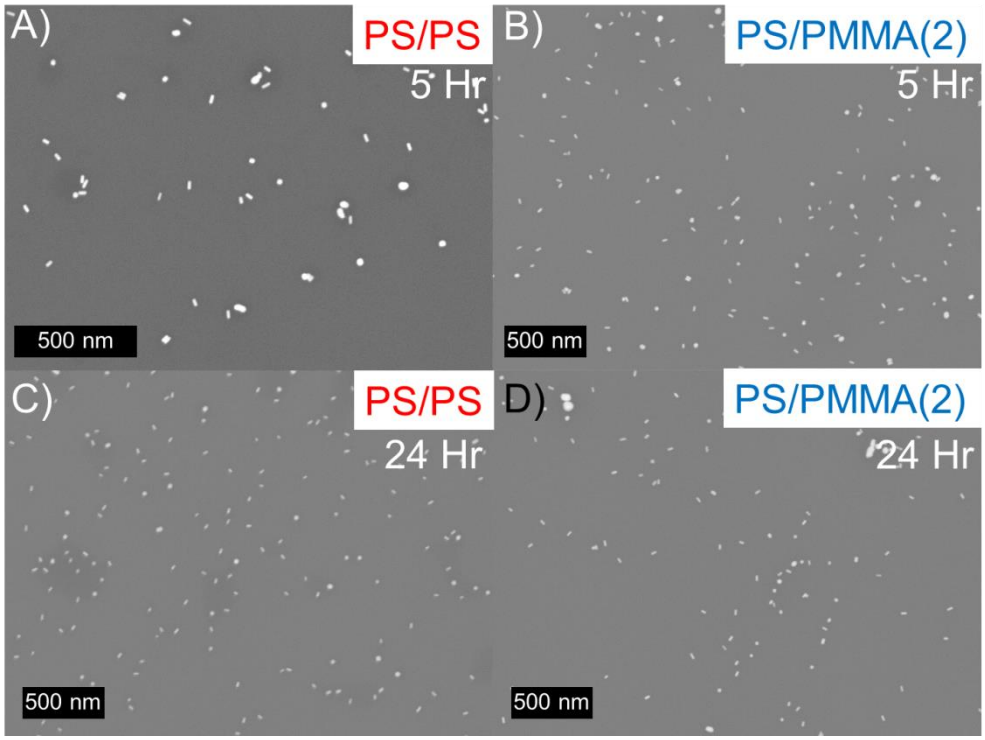

Figure S8: SEM image of the nanocomposite samples after annealing at 473 K for 5 hours (A, B) and 24 hours (C, D) for the PS/PS (left column) and PS/PMMA (2) (right column) samples. The AuNRs have mostly converted to spheres, and are well dispersed in the sample.

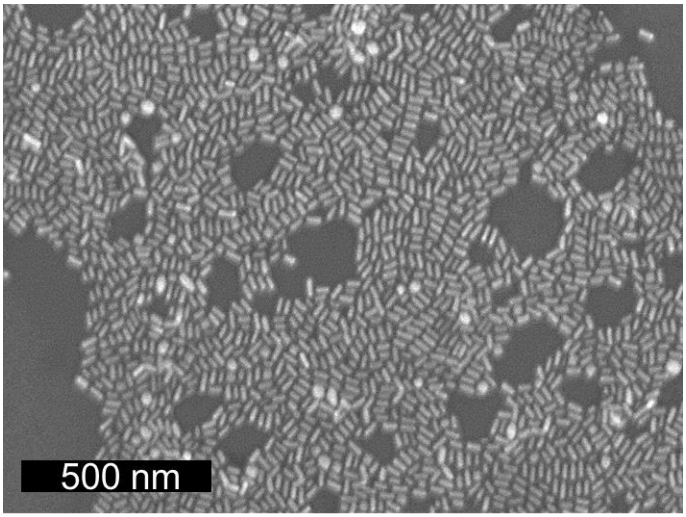

Figure S9: SEM image of PS grafted AuNRs on baser silicon, used to calculate the size distribution of the particles.

1. Jackson, J. D., *Classical Electrodynamics*. 2nd ed.; John Wiley & Sons Inc: New York, 1975.
2. Hastings, S. P.; Swanglap, P.; Qian, Z. X.; Fang, Y.; Park, S. J.; Link, S.; Engheta, N.; Fakhraai, Z. *Acs Nano* **2014,** 8, (9), 9025-9034.
3. Sanchez-Gaytan, B. L.; Qian, Z. X.; Hastings, S. P.; Reca, M. L.; Fakhraai, Z.; Park, S. J. *Journal of Physical Chemistry C* **2013,** 117, (17), 8916-8923.
4. Haynes, W. M., *CRC Handbook of Chemistry and Physics*. 96th ed.; CRC Press: Florida, 2015.
5. Papas, C. H., *Theory of Electromagnetic Wave Propagation*. Dover Publications, Inc.: New York, 1988.
6. Ishimaru, A., *Electromagnetic Wave Propagation, Radiation, and Scattering*. Prentice Hall: New Jersey, 1991.